Optically Distributing Remote Two-Node Microwave Entanglement Using Doubly Parametric Quantum Transducers

Akira Kyle,[1,2,†] Curtis L. Rau,[1,2,†] William D. Warfield,[1,2] Alex Kwiatkowski,[1,2] John D. Teufel,[2] Konrad W. Lehnert,[1,2,3] and Tasshi Dennis[2,*]

[1] *Department of Physics, University of Colorado, Boulder, Colorado 80309, USA*
[2] *National Institute of Standards and Technology (NIST), Boulder, Colorado 80305, USA*
[3] *Joint Institute for Laboratory Astrophysics (JILA), University of Colorado and National Institute of Standards and Technology (NIST), Boulder, Colorado 80309, USA*

(Received 28 December 2022; revised 7 April 2023; accepted 26 May 2023; published 6 July 2023)

Doubly parametric quantum transducers (DPTs), such as electro-optomechanical devices, show promise as quantum interconnects between the optical and microwave domains, thereby enabling long-distance quantum networks between superconducting qubit systems. However, any transducer will inevitably introduce loss and noise that will degrade the performance of a quantum network. We explore how DPTs can be used to construct a network capable of distributing remote two-mode microwave entanglement over an optical link by comparing 14 different network topologies. The 14 topologies we analyze consist of combinations of different transducer operations, entangled resources, and entanglement-swapping measurements. For each topology, we derive a necessary and sufficient analytic threshold on DPT parameters that must be exceeded in order to distribute microwave-microwave entanglement. We find that the thresholds are dependent on the given network topology, along with the available entanglement resources and measurement capabilities. In the high-optical-loss limit, which is relevant to realistic networks, we find that down-conversion of each half of an optical two-mode squeezed vacuum state is the most robust topology. Finally, using currently achievable experimental capabilities, we find the encouraging result that several of these topologies could produce microwave-microwave entanglement. However, most of these topologies cannot work given current transducer performance, which demonstrates the importance of thoroughly analyzing all possible networks.

DOI: 10.1103/PhysRevApplied.20.014005

I. INTRODUCTION

An outstanding challenge of superconducting quantum systems operating in the microwave regime is to interface them with optical photons, which is crucial for enabling the quantum networking of superconducting quantum processors [1]. Thus microwave-optical (MO) quantum transducers that preserve quantum coherence between the optical and microwave domains are required. Existing transducers are quickly improving as sources of decoherence, such as noise and loss, fall below optical-microwave separability and positive-partial-transpose- (PPT) preserving thresholds that define quantum operation [2]. The next step is to then understand how best to interconnect *two* transducers in order to form an optically linked quantum network between two microwave systems.

Given that transduction devices will likely be the limiting elements in near-term demonstrations of quantum networks, we should identify network topologies that place the least stringent demands on the transducers, by allowing the networks to make use of, e.g., ancillary resource states and measurements. We explore this question by evaluating a variety of possible network topologies that generate two-mode microwave entanglement using two transducers and experimentally realizable Gaussian entanglement resources and measurements. We focus on doubly parametric transducers (DPTs), such as electro-optomechanical devices, which have recently been used to optically read out the state of a superconducting qubit [3,4].

Previous work has proposed and analyzed single networks that use two transducers to accomplish either state transfer [5,6] or entanglement [7–9] between two qubits operating at microwave frequencies over an optical link. References [10–12] have also each analyzed a

*tasshi.dennis@nist.gov
†These authors contributed equally

single network for entangling two continuous-variable (CV) microwave modes. In this work, we analyze a set of *fourteen* different network topologies and compare their abilities to entangle CV microwave modes using two DPTs. The final microwave-microwave (MM) states produced by the networks we analyze are all 1×1 bipartite Gaussian states with so-called *balanced correlations* [13]. This is the class of states that are equivalent, up to local unitaries on each mode, to the two-mode squeezing of thermal states. By focusing on the generation of entanglement, rather than the transfer of arbitrary quantum states with high fidelity, we are able to provide necessary and sufficient entanglement thresholds for the transducer parameters and loss beyond which the network becomes separable across the two microwave modes and hence would be no better than a classical network. Additionally, by focusing on CV entanglement, we do not need to specify the protocol for interconnecting qubit systems with the inherently CV transduction channel, although we note that such protocols have been proposed [8,14].

To optimize and compare quantum networks, a metric must be chosen to quantify the ability of the network to accomplish some set of tasks. As we are concerned with the ability of a network to produce entangled MM states, we naturally choose an entanglement measure as our metric [15]. Unfortunately, even for the relatively simple class of two-mode Gaussian states, different entanglement measures may induce different orderings on the set of entangled states [16]. Thus, differing choices of entanglement measures will potentially lead to differing optimal network-parameter values and topologies. For the balanced-correlation states that we analyze, logarithmic negativity and entanglement of formation induce the same ordering on the set of entangled states [16]. For convenience, we quantify entanglement using logarithmic negativity, which is a necessary and sufficient condition for separability of $1 \times N$ bipartite Gaussian states. However, in general, entanglement measures need only give necessary conditions for separability [17]. Logarithmic negativity is an upper bound on distillable entanglement, which is one of the most relevant metrics for tasks involving quantum networks where entanglement is often the limiting resource, as opposed to local operations and classical communication [18]. Finally, while distillable entanglement and entanglement of formation are typically difficult to compute, logarithmic negativity can be easily computed analytically (for details, see Appendix E).

The network-entanglement thresholds we find constitute necessary and sufficient conditions for the final MM states to be entangled. The network-entanglement thresholds are a function of the parameters that characterize the two DPTs along with the other network components. We find the entanglement threshold for each network in order to discern which networks impose the least stringent requirements on the DPT parameters that must be experimentally realized. We furthermore evaluate the logarithmic negativity of the generated MM states for currently achievable DPT parameter values, finding that four topologies show potential for generating remote MM entanglement using recently demonstrated transducers. We find that there exist striking differences in how each network tolerates imperfections [e.g., most (10 out of 14) topologies cannot be successfully implemented with current transducers], which demonstrates the importance of comparing many experimentally feasible network topologies.

II. DOUBLY PARAMETRIC TRANSDUCER MODEL OVERVIEW

In this section, we briefly review the DPT model and approximations that allow the transducer to be described as a two-mode Gaussian bosonic channel. For a more detailed description, see Ref. [2, Sec. II and Appendix A]. DPTs consist of a mediating bosonic resonator mode coupled to optical and microwave bosonic resonator modes. The optical and microwave resonators are each coupled to bosonic itinerant input and output modes. Additionally, all three resonator modes are coupled to environmental baths, which we assume to have negligible thermal occupancy at the microwave and optical frequencies but n_{th} thermal phonons at the frequency of the mediating mode. The strong coherent-state pumps parametrically enhance the relatively weak bare-coupling rates to the mediating mode and provide the energy difference needed to bridge the gap between optical and microwave domains while preserving quantum coherence. After making the resolved sideband approximation and only considering the frequency modes that are on resonance with their respective optical and microwave resonators, the linear input-output relations between itinerant modes can be captured by five dimensionless quantities. The cooperativities $C_{\{a,b\}}$ give the rate at which information is coupled between the respective optical or microwave mode and the mediating mode relative to the rate at which it decays to the environment. The subscript a refers to an optical parameter, while the subscript b refers to a microwave parameter. The transmissivity parameters $\tau_{\{a,b\}}$ account for coupling inefficiency due to internal cavity losses and thus describe how undercoupled or overcoupled the optical and microwave itinerant modes are to their respective cavity modes ($\tau_{\{a,b\}} = 1$ corresponds to the ideal limit of no internal losses and thus completely overcoupled). In general, this coupling loss behaves differently than other losses (e.g., transmission losses or mode-matching losses) that are introduced in Sec. III D.

By tracing out the environment, we reduce the input-output relations to a two-mode Gaussian bosonic channel characterized by two 4×4 matrices, $\mathbf{T}$ and $\mathbf{N}$ (the explicit forms of which are given in Appendix A). This channel acts on the covariance matrix of an input MO state as

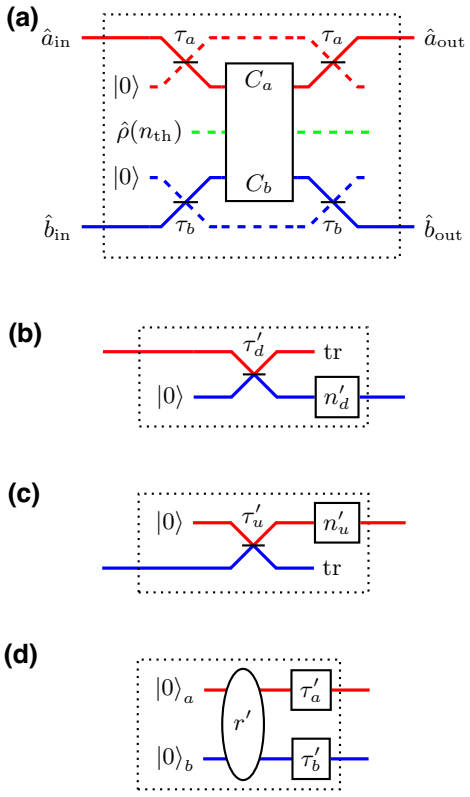

FIG. 1. (a) A circuit representing the optical-microwave input-output relations of a DPT, where the optical, microwave, and mediating modes are shown in red, blue, and green, respectively. The solid lines correspond to accessible itinerant modes, while the dashed lines correspond to environmental modes. This circuit reduces to the basic components shown in (b)–(d), which we use to construct our network topologies. (b) The single-mode down-conversion channel obtained by initializing the microwave input in a vacuum state and tracing out the optical output. (c) The single-mode up-conversion channel obtained by initializing the optical input in a vacuum state and tracing out the microwave output. (d) The effective circuit for a DPT under a squeezing-type interaction with vacuum inputs, which generates a two-mode squeezed lossy state. An ellipse denotes a two-mode squeezing operation. The effective channels shown in (b)–(d) are completely characterized by the effective transmissivities $\tau'_{\{u,d\}}$ and $\tau'_{\{a,b\}}$, the added noise $n'_{\{u,d\}}$, and the squeezing r' (explicit forms are given in Ref. [2]).

$\mathbf{V} \to \mathbf{TVT}^\top + \mathbf{N}$ [19]. The matrices $\mathbf{T}$ and $\mathbf{N}$ are functions of the five dimensionless parameters introduced above: $C_{\{a,b\}}$, $\tau_{\{a,b\}}$, and $n_{\rm th}$. This channel is illustrated with an effective circuit diagram in Fig. 1(a), where the MO input and output modes are represented by the operators $\hat{a}_{\rm in}, \hat{b}_{\rm in}$ and $\hat{a}_{\rm out}, \hat{b}_{\rm out}$, respectively.

The detuning of the coherent MO pumps relative to their respective resonators determines the nature of the interaction that the DPT implements. Red detuning by the frequency of the mediating mode maximizes anti-Stokes scattering with the mediating mode, while blue detuning by the frequency of the mediating mode maximizes Stokes scattering with the mediating mode. Thus when both pumps are red detuned, the device implements a beam-splitter-type interaction between microwave and optical modes. Whereas when one pump is red detuned and the other pump is blue detuned, the device implements a two-mode squeezing-type interaction between microwave and optical modes. In our previous work, we have characterized the fundamental separability thresholds of the channel of the transducer under both types of interactions [2]. The linearized equations of motion are always stable for the beam-splitter-type interaction; however, the squeezing-type interaction is subject to stability conditions that can be found using the Routh-Hurwitz criteria [20,21]. For the exact form of these stability criteria, see Eqs. (B1) and (B2).

III. CONSTRUCTING NETWORKS

A. The basic network components

We now construct the set of network topologies that we analyze. The objective of the networks we construct is to entangle two remote microwave modes that can only be connected via an optical channel. Thus we immediately see that the networks will require two transducers that are each colocated with the remote microwave modes to be entangled. Additionally, the network will need a source of MO entanglement, which can be produced "intrinsically" within the transducers themselves when operating under the squeezing-type interaction or via "extrinsic" sources generated separately in either the microwave or optical domain.

To simplify the set of networks we consider, we first restrict how the transducers can operate within the network. We consider only accessing either the input or output of the transducer in the microwave domain and likewise for the optical domain. Any unused inputs are initialized in vacuum, while any unused outputs are discarded (traced). Thus a transducer can be used as a one-mode up-converter [Fig. 1(b)] or down-converter [Fig. 1(c)] when both pumps are red detuned or as a source of entanglement [Fig. 1(d)] when one pump is red and the other blue detuned. The two possibilities give rise to an effective Hamiltonian of $\hat{a}^\dagger\hat{c}^\dagger + \hat{b}\hat{c}^\dagger + \text{h.c.}$ for a blue-detuned optical pump or $\hat{a}\hat{c}^\dagger + \hat{b}^\dagger\hat{c}^\dagger + \text{h.c.}$ for a blue-detuned microwave pump, where $\hat{c}$ denotes the mediating bosonic mode.

We restrict the set of resource states, channels, and measurements to be Gaussian, to make the subsequent analysis analytically tractable and since these are the most readily available experimentally. Within the Gaussian restriction, the resource states we consider are two-mode squeezed (TMS) states. Additionally, we allow for joint measurements on two modes and conditional unitaries in order for the networks to accomplish entanglement-swapping protocols. The specific joint measurement we allow for is

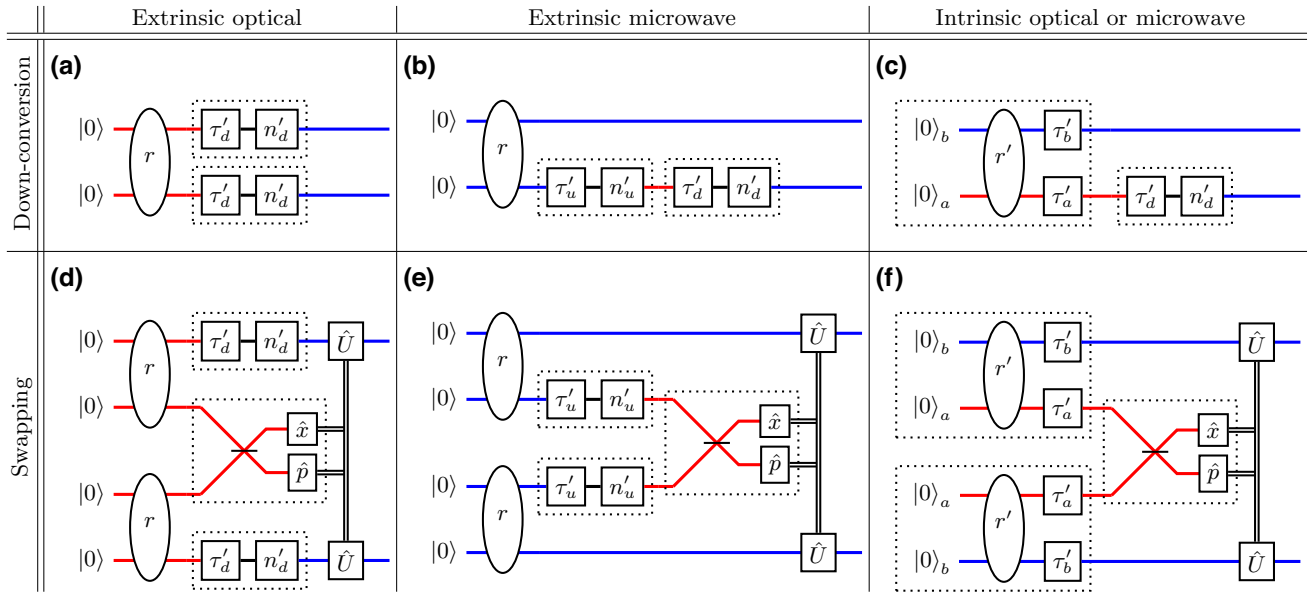

FIG. 2. Diagrams of the microwave-microwave entanglement distribution networks that we analyze: (a)–(c) represent down-conversion networks while (d)–(f) represent swapping networks. In (a) and (d), entanglement is generated extrinsically in the optical domain. In (b) and (e), entanglement is generated extrinsically in the microwave domain. In (c) and (f), entanglement is generated intrinsically in the transducer, where the optical or microwave label refers to whether the optical or microwave pump is blue detuned. As in Fig. 1, the optical and microwave modes are shown in red and blue, respectively. The length of lines in these diagrams do not correspond to physical transmission lengths.

projection onto two-mode states with infinite squeezing, which is optically accomplished by combining each mode on a balanced beam splitter and then making opposite quadrature measurements. This measurement is sometimes referred to as a CV-Bell or an EPR measurement. Allowing additional Gaussian components is unlikely to signicantly improve a network and in practice will often be worse due to introducing additional sources of decoherence that cannot be corrected for, since entanglement distillation is impossible using only Gaussian operations [22–24]. Therefore, we consider the simplest possible networks that accomplish the desired task.

B. The network topologies

To build our set of network topologies, we first enumerate the set of ways to create MO entanglement using the allowed components and when the resulting MO state is entangled [2]:

(1) *Extrinsic optical (EO)*. Generate a TMS optical state and down-convert one mode to microwave using the transducer as in Fig. 1(b). The resulting MO state is entangled if and only if $n_{\text{th}} < \tau_a C_a$.

(2) *Extrinsic microwave (EM)*. Generate a TMS microwave state and up-convert one mode to optical using the transducer as in Fig. 1(c). The resulting MO state is entangled if and only if $n_{\text{th}} < \tau_b C_b$.

(3) *Intrinsic optical (IO)*. Use the transducer to produce a two-mode squeezed lossy state as in Fig. 1(d), with the optical pump blue detuned. The resulting MO state is always entangled.

(4) *Intrinsic microwave (IM)*. Use the transducer to produce a two-mode squeezed lossy state as in Fig. 1(d), with the microwave pump blue detuned. The resulting MO state is always entangled.

Next, we consider two classes of topologies—down-conversion and swapping—that convert the MO entanglement into the final MM entanglement. The set of down-conversion topologies is shown in Figs. 2(a)–2(c), where the optical mode of a MO state is down-converted using the transducer operating as in Fig. 1(b). In the set of swapping topologies, a joint EPR measurement is performed on the two optical modes of two MO states. The measurement outcomes are then used to implement a conditional displacement, which then potentially entangles the remaining MM state. Given our four MO resource states, there are then four down-conversion topologies and ten swapping topologies allowed. The swapping topologies can be further subdivided into four symmetric swapping topologies (where the two MO resource states are generated in the same way) and six asymmetric swapping topologies (where the two MO resource states are generated in different ways). Thus we construct 14 network topologies. The set of four symmetric swapping topologies is shown in Figs. 2(d)–2(f). The asymmetric swapping topologies are

not explicitly shown in Fig. 2 but for clarity we give one example, which is illustrated in Fig. 6 where we use the extrinsic optical and intrinsic microwave methods to generate two MO states and then measure the optical modes of these two states to perform entanglement swapping.

C. Nonoptimality of asymmetric entanglement swapping

We conclude that the six asymmetric swapping topologies are never optimal by showing the following theorem. For the proof of this theorem and the definition of balanced-correlated Gaussian states, see Appendix G.

Theorem.—Let $\mathbf{V}_1 \neq \mathbf{V}_2$ be the covariance matrices of two distinct two-mode balanced-correlated Gaussian states. After performing a joint EPR measurement on the first mode of each of the two states, let the logarithmic negativity of the resulting state be E_{ij} where $i,j \in \{1,2\}$ index which states are used in the swapping protocol. Then, we have that

$$E_{12} \leq \max\{E_{11}, E_{22}\}. \tag{1}$$

This theorem allows us to exclude asymmetric swapping topologies from further consideration, since a symmetric swapping topology will always perform better, both in terms of having a lower network-entanglement threshold and in the amount of entanglement produced. The remainder of this paper is dedicated to comparing the four distribution topologies and four symmetric swapping topologies, which are explicitly drawn in Fig. 2.

D. Optimizing networks

The logarithmic negativity should be optimized over the experimentally accessible free parameters. We do not require the two transducers to be operated with the same set of values for the dimensionless parameters ($C_{\{a,b\}}$, $\tau_{\{a,b\}}$, and n_{th}). Rather, we should consider that both transducers have the same maximum achievable values (or minimal in the case n_{th}) and that it is easy to independently reduce (increase) the parameters from their maximal (minimal) values in an experiment. We set $\tau_{\{a,b\}}$ equal to their maximum possible values and n_{th} equal to the minimum possible value for each transducer, which we conjecture will always maximize the MM-state logarithmic negativity. This allows us to eliminate three parameters from the set of parameters that characterize the network (since now $\tau_{\{a,b\}}$ and n_{th} are equal for both transducers). In contrast, we find that it is not always optimal to set all cooperativities to their maximum values. For example, increasing the optical cooperativity to be larger than the microwave cooperativity causes the effective down-conversion transmissivity (given by Eq. (A6)) to decrease and can result in less MM entanglement. Thus, we must carry out an optimization procedure over all four cooperativities. Namely, we maximize logarithmic negativity for each topology subject to the constraints that $0 \leq C_{a,i} \leq D_a$ and $0 \leq C_{b,i} \leq D_b$, where $i = 1,2$ indicates the transducer, while $D_{\{a,b\}}$ are the maximum achievable optical and microwave cooperativities (see Appendix E). Recall that the squeezing-type interaction is subject to stability constraints, which must also be taken into account when performing this optimization over the four cooperativities (see Appendix B).

Thus far, we have not considered optical transmission loss, which could come from, e.g., absorption in optical fibers. Such external optical losses should also be included in the optimization procedure, as there is often experimental freedom in how the optical loss is distributed between as many as four optical modes, as can be seen in Fig. 2. For the extrinsic microwave down-conversion and the two intrinsic down-conversion topologies, there is only one optical mode and so the optimization is trivial. In the case of extrinsic optical down-conversion and swapping, splitting all transmission losses equally between the two down-converted modes is optimal, which we show in Appendix H 1. For these five topologies then, the external optical transmission loss $1-\tau_e$ is optimally distributed by simply taking $\tau_a \to \sqrt{\tau_e}\tau_a$. However, for the remaining nine swapping topologies there remains a complex optimization problem over four cooperativities and the external optical transmission loss distribution. Unfortunately, the introduction of transmission loss means that the result in Appendix G can no longer be used to eliminate the asymmetric swapping topologies from consideration. Thus, a simultaneous optimization over cooperatives and transmission loss must be carried out over the entire set of 14 topologies in order to find the optimal network topology. We further discuss several results of this optimization over external optical transmission loss in more detail in Appendix H. For example, in Appendix H 2, we show that in the limited case of swapping two identical MO states (which is relevant to the extrinsic microwave and intrinsic optical or microwave swapping topologies), it is optimal to distribute this loss completely onto one of the optical modes after transduction.

IV. NETWORK-ENTANGLEMENT THRESHOLDS

To identify promising network topologies, we examine the thresholds on the transducer and network parameters that must be exceeded for the final MM state to be entangled. The network-entanglement thresholds are found by first computing the covariance matrices of the four MO states (see Appendix C), which are then used to calculate the covariance matrix of the resulting MM states (see Appendix D). From the MM covariance matrix, we can calculate the logarithmic negativity, which we set equal to zero and solve for n_{th}. This procedure then yields the threshold. The MM state is entangled if and only if n_{th} is less than this threshold; thus the network-entanglement

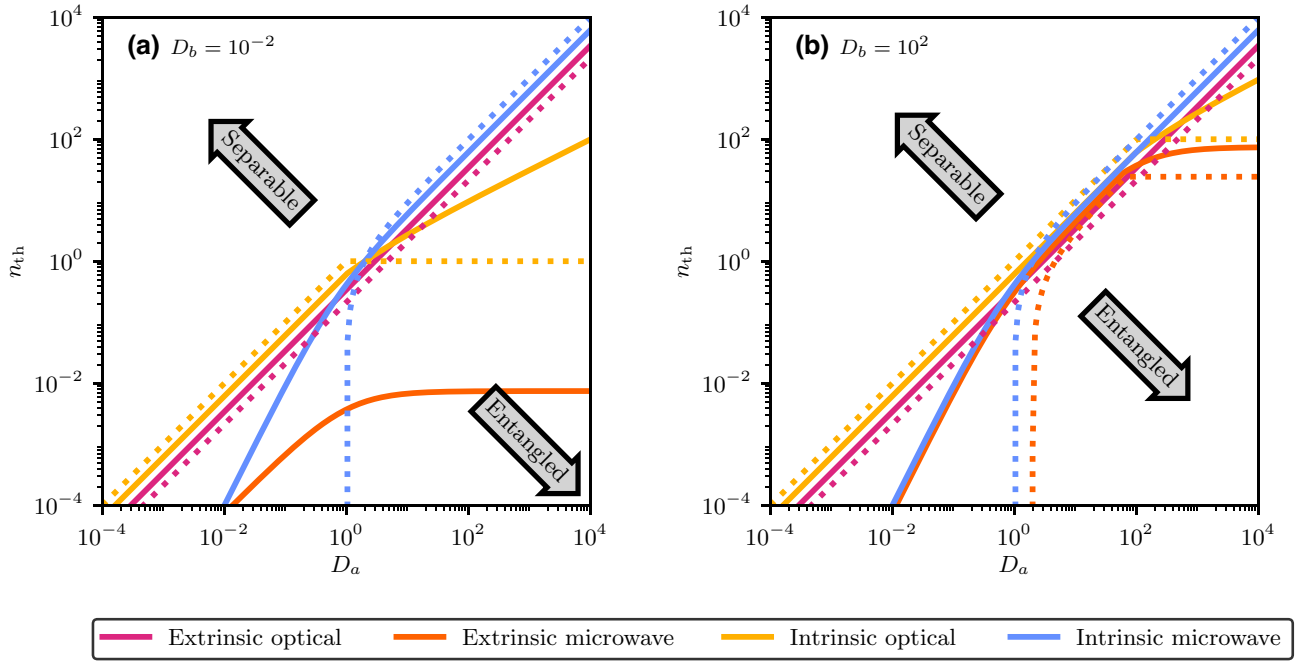

FIG. 3. Plots of the network-entanglement thresholds in Table I, which correspond to the network topologies shown in Fig. 2. The microwave-microwave state created by each network topology is entangled below its corresponding curve and separable in the region above. The solid curves represent down-conversion thresholds, while the dotted curves represent swapping thresholds. These plots illustrate differences between networks when the limiting factors are noise from the thermal bath of the mediating mode and finite cooperativities. Here, we set $\tau_a = 1$, $\tau_b = 0.75$, and $r = 0.58$ (i.e., 5 dB of extrinsic squeezing). For the topologies that depend on C_b (both extrinsic microwave topologies), we set C_b to the value that maximizes the threshold on n_{th}. In (a), the extrinsic microwave swapping MM state is always separable for $D_b = 10^{-2}$.

thresholds are upper bounds on n_{th}. Table I gives these upper bounds on n_{th} for each of the eight topologies shown in Fig. 2. A notable feature of these thresholds is that only the extrinsic microwave swapping and down-conversion topologies explicitly depend on any microwave parameters (D_b and τ_b). However, the microwave cooperativity implicitly affects the intrinsic optical thresholds through the stability constraints.

The network-entanglement thresholds are plotted in Figs. 3 and 4. For each topology, the corresponding curve delineates the boundary between a separable (above) or entangled (below) MM state. In Fig. 3, we see the effect of cooperativity imbalances in limiting the thresholds as a result of the optimization procedure, with the notable exception of the extrinsic optical topologies, the thresholds of which are only dependent on τ_a, D_a, and r and hence insensitive to cooperativity imbalance. In the high-optical-loss regime of Fig. 4, the threshold scales linearly with loss only for the extrinsic optical topologies, while the rest scale quadratically, indicating that for large optical losses, the extrinsic optical topologies are the only feasible candidates for attempting to create MM entanglement (for further discussion of relevant features of these thresholds, see Appendix F).

Some features of these thresholds can be understood in terms of general results that have been found previously. Recently, Ref. [25] has proved that all joint Gaussian measurements are separable when the average loss on the two

TABLE I. The network-entanglement thresholds that are necessary and sufficient conditions for entanglement of the microwave-microwave state created by each network topology shown in Fig. 2. These expressions are an upper bound on the thermal-bath occupancy of the mediating mode. When n_{th} is less than one of these thresholds, the corresponding MM state is entangled. $\bar{C}_a$ indicates that this cooperativity should be maximized while still satisfying the stability constraints for a blue-detuned optical pump. For the extrinsic microwave down-conversion and swapping topologies, the expressions for the upper bounds on n_{th} that are optimized over cooperativities are not simple, so we do not give the explicit expressions here.

	Down-conversion	Swapping
EO	$\frac{\tau_a D_a \left(1 - e^{-2r}\right)}{2}$	$\tau_a D_a \frac{\sinh^2(r)}{\cosh(2r)}$
EM	$\frac{4\tau_a^2 \tau_b C_a C_b D_a}{(1 + C_a + C_b)^2 + 4\tau_a^2 C_a D_a}$	$\tau_b C_b - \frac{(1 + C_a + C_b)^2}{8\tau_a C_a}$
IO	$\frac{\sqrt{\bar{C}_a(\bar{C}_a + 4\tau_a^2 D_a)} - \bar{C}_a}{2}$	$(2\tau_a - 1)\,\bar{C}_a$
IM	$\frac{\sqrt{(1 + D_a)^2 + 4\tau_a^2 D_a^2} - D_a - 1}{2}$	$(2\tau_a - 1)\,D_a - 1$

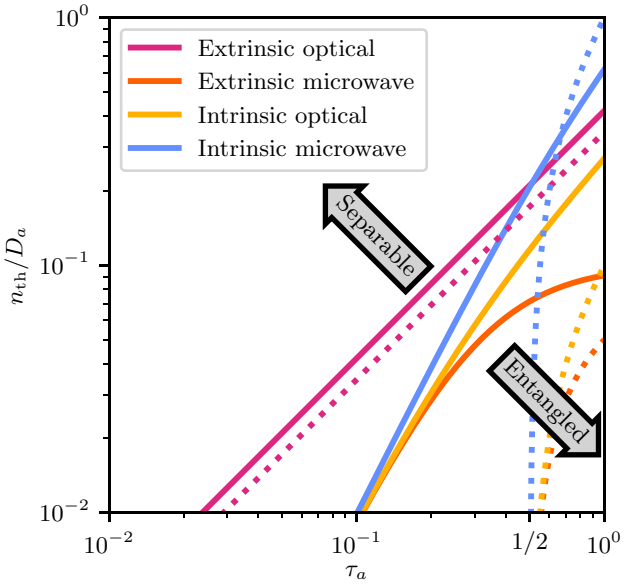

FIG. 4. A plot of the network-entanglement thresholds in Table I, which correspond to the network topologies shown in Fig. 2. The microwave-microwave state created by each network topology is entangled below its corresponding curve and separable in the region above. The solid curves represent down-conversion thresholds, while the dotted curves represent swapping thresholds. This plot illustrates the differences in tolerance to optical loss between the networks when cooperativities are high. Here, we set $D_a = 10D_b \gg 1$, $\tau_b = 1$, and $r = 0.92$ (i.e., 8 dB of extrinsic squeezing). In the limit of $D_b \gg D_a$, the extrinsic microwave down-conversion and intrinsic optical down-conversion thresholds become identical to the intrinsic microwave down-conversion threshold and likewise for the swapping thresholds. For the topologies that depend on C_b (both extrinsic microwave topologies), we set C_b to the value that maximizes the threshold on $n_{\rm th}$.

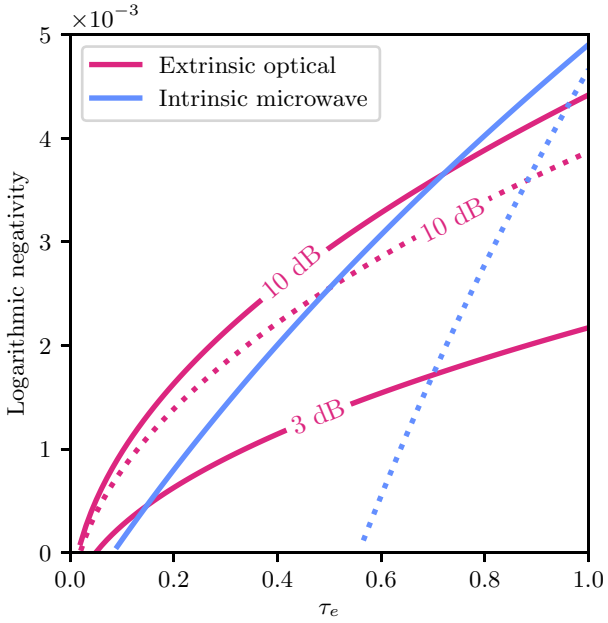

FIG. 5. The logarithmic negativity of the final microwave-microwave state generated by each network topology using recently reported electro-optomechanical-transducer parameter values plotted as a function of optical loss external to the transducer (such as transmission and measurement losses) [3,27]. Topologies that are not shown here do not produce microwave-microwave entanglement for these parameter values. The solid lines indicate down-conversion topologies, while the dotted lines indicate swapping topologies. For the extrinsic optical topologies, we include lines for 3 dB and 10 dB of extrinsic squeezing. The transducer parameter values are taken directly from Ref. [2].

optical modes exceeds 1/2. This requires the swapping topologies to be separable when $\tau_a < \frac{1}{2}$, with the exception of the extrinsic optical swapping topology, where τ_a does not affect the measured modes. The extrinsic optical down-conversion and swapping topologies are effectively the same, since a lossless EPR measurement on two pure TMS states results in a pure TMS state with reduced squeezing [26]. Note that all thresholds in Table I are less than or equal to $\tau_a D_a$, indicating that $n_{\rm th} < \tau_a D_a$ is a global necessary condition for producing MM entanglement. For the down-conversion topologies along with the extrinsic optical swapping topology, this is simply a consequence of the entanglement-breaking threshold of the one-mode down-conversion channel [2].

V. PROSPECTS FOR NEAR-TERM QUANTUM NETWORKS

We find that current DPTs show potential for generating remote two-node MM entanglement over an optical link. A recent experiment has reported the operation of an electro-optomechanical device with parameter values $D_a = 26\,000$, $D_b = 124$, $n_{\rm th} = 1000$, $\tau_a = 0.791$, $\tau_b = 0.866$, $\delta_a = \epsilon_a = 0.88$, and $\delta_b = \epsilon_b = 0.34$ (where $\delta_a = \epsilon_a$ are the transmissivities representing optical mode-matching and $\delta_b = \epsilon_b$ are the transmissivities representing microwave transmission loss [2,3,27].) We incorporate these parameters and the optical transmission loss $(1 - \tau_e)$ by redefining $\tau_{\{a,b\}}$ to be $\tau_a\delta_a\sqrt{\tau_e} = \tau_a\epsilon_a\sqrt{\tau_e}$ and $\tau_b\delta_b = \tau_b\epsilon_b$. This equally distributes the optical transmission loss between the two optical modes just before or after transduction, although as discussed in Sec. III D, this is only optimal for the down-conversion and extrinsic optical swapping topologies. Figure 5 uses these values to plot the logarithmic negativity of the MM state produced by each network topology as a function of the external optical transmissivity τ_e and includes lines for 3 dB and 10 dB of extrinsic squeezing.

Of the 14 topologies we consider in the previous section, only four are capable of producing MM entanglement for the reported transducer parameter values. The topologies capable of MM entanglement are the extrinsic optical topologies that have superior performance

under large optical transmission loss and the intrinsic microwave topologies that perform better under limited optical transmission loss. The down-conversion version of these topologies always outperforms the swapping version for these parameter values, since the amount of optical coupling loss ($\tau_a = 0.791$) inherent to the transducer limits the effectiveness of the CV swapping measurement, even in the limit of no optical transmission loss. In Fig. 5, we see that the logarithmic negativity of the MM states can differ significantly between the topologies, depending on the amount of external optical loss that may be incurred. This illustrates the importance of carefully optimizing and then selecting the network topology based on achievable transducer- and network-parameter values. There can be a number of viable network topologies and the differences in entanglement between them can be significant. Meanwhile, many network topologies may not even be viable.

We can estimate an upper bound on the distillable MM entangled-bit rates that could potentially be generated using these transducers by multiplying the logarithmic negativity by the bandwidth of the device (which is approximately 2 kHz). Assuming a typical fiber loss rate of 0.18 dB/km at 1550 nm, we see from Fig. 5 that for $\tau_e = 0.9$, corresponding to approximately 2 km of fiber, the intrinsic microwave down-conversion topology would have a maximum entangled-bit (e-bit) rate of approximately 6 e-bits per second.

VI. CONCLUSIONS

We find the entanglement thresholds on DPT parameters in order to distribute MM entanglement for a set of eight network topologies, while eliminating a set of six asymmetric swapping topologies since they are always inferior. We find that among the set of networks we analyze, there is not a unique topology that is universally optimal with respect to separability or the logarithmic negativity entanglement measure. The best network is dependent on the achievable DPT parameter values, where an optimization must be carried out over the cooperativity values of each transducer and over the distribution of the optical transmission loss between the optical modes.

We found that with respect to network-entanglement thresholds, the intrinsic swapping topologies have the least restrictive thresholds in the low-optical-loss limit (i.e., short distances and small optical coupling losses). Conversely, in the high-optical-loss limit (i.e., long distances and/or large optical coupling losses), the extrinsic optical down-conversion topology has the least restrictive threshold. This can be intuitively understood by observing that the extrinsic optical down-conversion topology can equally distribute optical loss onto two modes instead of all loss occurring on a single mode, as is the case for the other down-conversion topologies. Meanwhile, the swapping topologies are subject to the average optical loss threshold of $1/2$ for separability, which is proven Ref. [25].

For recently achieved DPT parameter values, we calculate the logarithmic negativity of the MM state that each network topology is capable of creating. We find that, similar to the separability thresholds, the network-parameter values dictate which network topology will produce the most entanglement and that the differences in the amount of entanglement produced by different network topologies can be significant. Thus, knowing which network topology to use when operating in different parameter regimes will be essential for building the most effective near-term quantum network capable of entangling superconducting qubits.

While our analysis considers many possible network topologies, we limit the possible operating modes of the transducer to just single-mode up-conversion and down-conversion in addition to two-mode microwave-optical squeezing. Our previous work in Ref. [2] shows that considering the transducer as a *two-mode* Gaussian quantum channel allows for quantum operation to be achieved under less restrictive transducer parameter values. Possible future work would consider network topologies that utilize both the microwave and optical inputs and outputs of the two transducers in a single network topology, where we would expect improvements beyond the global necessary condition $n_{\text{th}} < \tau_a D_a$ that all the networks considered here must satisfy. For example, the extrinsic optical down-conversion and extrinsic microwave swapping topologies could be simultaneously implemented with two transducers. Furthermore, allowing non-Gaussian states, channels, and measurements would very likely allow network topologies that are far less restrictive by utilizing, for example, distillation, concentration, or purification protocols or bosonic error-correction codes. As the ultimate goal is to entangle qubits, the networks will naturally have access to the non-Gaussian resources of the quantum processors that they connect. The interface between the CV modes of the transducer to the qubits of the quantum processors may potentially look like a distillation protocol, a bosonic code, or some hybrid between the two. Thus, understanding the optimal way to accomplish this interface will both affect and be affected by the network topology that connects the quantum processors.

ACKNOWLEDGMENTS

We would like to thank Ezad Shojaee, Emanuel Knill, Scott Glancy, Shawn Geller, Krister Shalm, and Ari Feldman for helpful suggestions and discussions. We acknowledge funding from the Army Research Office (ARO) Cross-Quantum Systems Science & Technology (CQTS) under Grant No. 67C1098620, the National Science Foundation (NSF) under Grant No. PHYS 1734006, and the NSF Quantum Leap Challenge Institutes (QLCI) under

Award No. OMA–2016244. At the time this work was performed, C.Rau, A. Kyle, and A. Kwiatkowski were supported as Associates in the Professional Research Experience Program (PREP) operated jointly by NIST and the University of Colorado Boulder under Award No. 70NANB18H006 from the U.S. Department of Commerce. This is a contribution of the National Institute of Standards and Technology, not subject to U.S. copyright.

APPENDIX A: GAUSSIAN DPT CHANNEL

As the starting point for this work, we adopt the same DPT model as used in Ref. [2]. As discussed in Sec. III, for any transducer, we only use either the input or output (but not both) in the optical domain and likewise for the microwave domain. When using a transducer in this way, the coupling losses τ_i, input losses δ_i, and output losses ϵ_i all affect the quantum channel of the DPT in the same way. Therefore, to reduce the number of parameters needed to characterize a DPT, we redefine $\tau_i\epsilon_i \to \tau_i$ or $\tau_i\delta_i \to \tau_i$ depending on how that port is used. For convenience, we make this substitution and then provide the explicit full form of $\mathbf{T}$ and $\mathbf{N}$, which are as follows:

$$\mathbf{T}_{\sigma_a,\sigma_b} = \frac{2}{1-\sigma_a C_a - \sigma_b C_b}\begin{pmatrix} \tau_a(1-\sigma_b C_b)\mathbf{I}_2 & \sqrt{\tau_a\tau_b C_a C_b}\begin{pmatrix}\sigma_a & 0\\ 0 & \sigma_b\end{pmatrix} \\ \sqrt{\tau_a\tau_b C_a C_b}\begin{pmatrix}\sigma_b & 0\\ 0 & \sigma_a\end{pmatrix} & \tau_b(1-\sigma_a C_a)\mathbf{I}_2 \end{pmatrix} - \mathbf{I}_4, \tag{A1}$$

$$\mathbf{N}_{\sigma_a,\sigma_b} = \frac{2}{(1-\sigma_a Ca - \sigma_b C_b)^2}\begin{pmatrix} \alpha\mathbf{I}_2 & \gamma\begin{pmatrix}\sigma_a\sigma_b & 0\\ 0 & 1\end{pmatrix} \\ \gamma\begin{pmatrix}\sigma_a\sigma_b & 0\\ 0 & 1\end{pmatrix} & \beta\mathbf{I}_2 \end{pmatrix}, \tag{A2}$$

$$\alpha = \tau_a\left[(1-\tau_a)(1-\sigma_b C_b)^2 + C_a(1+2n_{\rm th}+C_b(1-\tau_b))\right], \tag{A3}$$

$$\beta = \tau_b\left[(1-\tau_b)(1-\sigma_a C_a)^2 + C_b(1+2n_{\rm th}+C_a(1-\tau_a))\right], \tag{A4}$$

$$\gamma = \sqrt{\tau_a\tau_b C_a C_b}\left[2n_{\rm th} - \sigma_a\sigma_b(1+\sigma_b\tau_a+\sigma_a\tau_b + C_a(1-\tau_b)+C_b(1-\tau_a))\right], \tag{A5}$$

where σ_a and σ_b are the sign of the optical and microwave pumps, respectively (-1 for red-detuned, $+1$ for blue-detuned), and $\mathbf{I}_n$ is the $n \times n$ identity matrix. The above is true provided that at least one of the pumps is red detuned.

When both pumps are red detuned and we use the transducers as one-mode Gaussian conversion channels, we trace out the unused portion of the above channels. The up- and down-conversion one-mode channels are described by $\mathbf{T}_{\{u,d\}} = \sqrt{\tau_{\{u,d\}}}\mathbf{I}_2$ and $\mathbf{N}_{\{u,d\}} = n_{\{u,d\}}\mathbf{I}_2$, where

$$\begin{aligned}\tau_{\{u,d\}} &= -\frac{4\tau_a\tau_b C_a C_b}{(1+C_a+C_b)^2},\\ n_{\{u,d\}} &= \left(\frac{1}{2} + \frac{2\tau_{\{a,b\}}C_{\{a,b\}}(2n_{\rm th}-\tau_{\{b,a\}}C_{\{b,a\}})}{(1+C_a+C_b)^2}\right).\end{aligned} \tag{A6}$$

These expressions are closely related to Ref. [2, Eqs. (9) and (10)] (where here we have fixed the minor typographical errors that appear in the original equation).

APPENDIX B: STABILITY CRITERIA FOR BLUE-DETUNED PUMPS

There are two stability criteria for the linearized DPT model that we require to be satisfied whenever a DPT is operated as a two-mode squeezer [20]. One condition is

$$C_+ < C_- + 1, \tag{B1}$$

where the subscript $+$ refers to the mode with the blue-detuned pump and $-$ refers to the mode with the red-detuned pump.

The second stability criterion cannot be expressed in terms of the dimensionless transducer parameters. However, it can be expressed in terms of the enhanced couplings ($G_\pm$) and line widths ($\kappa_\pm$ and γ_m), which are explicitly defined in Ref. [2]. This stability criterion is given by Eq. 9a in Ref. [20, Appendix], which is reproduced here (with a minor typographical error that appears in the

original equation fixed):

$$\frac{\kappa_+ + \gamma_m}{\kappa_- + \gamma_m} < \frac{\kappa_- \gamma_m C_- + (\kappa_- + \kappa_+)(\kappa_+ + \gamma_m)}{\kappa_+ \gamma_m C_+} \tag{B2}$$

$$\Longrightarrow$$

$$\frac{4G_+^2}{\kappa_- + \gamma_m} < \frac{4G_-^2}{\kappa_+ + \gamma_m} + \kappa_+ + \kappa_-. \tag{B3}$$

APPENDIX C: COVARIANCE MATRICES FOR THE MICROWAVE-OPTICAL ENTANGLED STATES

In this appendix, we outline the procedure for calculating the covariance matrices of the four MO states that are introduced in Sec. III. We start by giving the explicit form of the input state into the transducer and the transformation that the transducer performs on this state for each case. Each of these MO states is produced by first initializing two modes in ether a two-mode squeezed vacuum state with covariance matrix

$$\mathbf{V}_{\mathrm{TMS}} = \frac{1}{2}\begin{pmatrix} \cosh(2r)\mathbf{I}_2 & \sinh(2r)\mathbf{Z}_2 \\ \sinh(2r)\mathbf{Z}_2 & \cosh(2r)\mathbf{I}_2 \end{pmatrix} \tag{C1}$$

or a vacuum state with covariance matrix

$$\mathbf{V}_{\mathrm{vac}} = \frac{1}{2}\,\mathbf{I}_4, \tag{C2}$$

where $\mathbf{Z}_2 = \mathrm{diag}(1, -1)$ is the Pauli Z matrix. The Gaussian-channel formalism allows us to easily evolve of these initial states through the network. All MO states are balanced-correlated two-mode states, which are characterized by a covariance matrix of the form

$$\mathbf{V}_i = \begin{pmatrix} a_i\,\mathbf{I}_2 & c_i\,\mathbf{Z}_2 \\ c_i\,\mathbf{Z}_2 & b_i\,\mathbf{I}_2 \end{pmatrix}, \tag{C3}$$

so the MO states are described by the three parameters a, b, and c. For our MO covariance matrices, we adopt the convention of the first mode being optical and the second mode being microwave. We also note that the extrinsic optical and microwave covariance matrices transform into one another by exchanging $a \leftrightarrow b$ and modes 1 and 2 and likewise for the intrinsic cases. The remainder of this appendix is dedicated to giving the explicit expressions for a, b, and c for each of the four MO states.

1. Extrinsic optical

Description. Start with an optical TMS state and down-convert the second mode (with a transducer where both pumps are red detuned):

$$\mathbf{V}_{\mathrm{EO}} = (\mathbf{I}_2 \oplus \mathbf{T}_d)\,\mathbf{V}_{\mathrm{TMS}}\,(\mathbf{I}_2 \oplus \mathbf{T}_d)^{\top} + 0\mathbf{I}_2 \oplus \mathbf{N}_d.$$

Covariance matrix:

$$\begin{aligned} a &= \frac{\cosh(2r)}{2}, \\ b &= \frac{1}{2} + \frac{2\tau_b C_b\,(2n_{\mathrm{th}} + \tau_a C_a(\cosh(2r) - 1))}{(1 + C_a + C_b)^2}, \\ c &= -\frac{\sqrt{\tau_a \tau_b C_a C_b}\,\sinh(2r)}{1 + C_a + C_b}. \end{aligned} \tag{C4}$$

2. Extrinsic microwave

Description. Start with a microwave TMS state and up-convert the first mode (with a transducer where both pumps are red detuned):

$$\mathbf{V}_{\mathrm{EM}} = (\mathbf{T}_u \oplus \mathbf{I}_2)\,\mathbf{V}_{\mathrm{TMS}}\,(\mathbf{T}_u \oplus \mathbf{I}_2)^{\top} + \mathbf{N}_u \oplus 0\mathbf{I}_2.$$

Covariance matrix:

$$\begin{aligned} a &= \frac{1}{2} + \frac{2\tau_a C_a\,(2n_{\mathrm{th}} + \tau_b C_b(\cosh(2r) - 1))}{(1 + C_a + C_b)^2}, \\ b &= \frac{\cosh(2r)}{2}, \\ c &= -\frac{\sqrt{\tau_a \tau_b C_a C_b}\,\sinh(2r)}{1 + C_a + C_b}. \end{aligned} \tag{C5}$$

3. Intrinsic optical

Description. Initialize both the optical and microwave inputs of the transducer in a vacuum state and use the transducer as an entanglement source with the optical pump blue detuned and the microwave pump red detuned:

$$\mathbf{V}_{\mathrm{IO}} = \mathbf{T}_{+-}\mathbf{V}_{\mathrm{vac}}\mathbf{T}_{+-}^{\top} + \mathbf{N}_{+-}. \tag{C6}$$

Covariance matrix:

$$\begin{aligned} a &= \frac{1}{2} + \frac{4\tau_a C_a\,(C_b + n_{\mathrm{th}} + 1)}{(1 - C_a + C_b)^2}, \\ b &= \frac{1}{2} + \frac{4\tau_b C_b\,(C_a + n_{\mathrm{th}})}{(1 - C_a + C_b)^2}, \\ c &= \frac{2\,(C_a + C_b + 2n_{\mathrm{th}} + 1)\,\sqrt{\tau_a \tau_b C_a C_b}}{(1 - C_a + C_b)^2}. \end{aligned} \tag{C7}$$

4. Intrinsic microwave

Description. Initialize both the optical and microwave inputs of the transducer in a vacuum state and use the transducer as an entanglement source with the optical pump red

detuned and the microwave pump blue detuned.

$$\mathbf{V}_{\mathrm{IM}} = \mathbf{T}_{-+}\mathbf{V}_{\mathrm{vac}}\mathbf{T}_{-+}^{\top} + \mathbf{N}_{-+}. \tag{C8}$$

Covariance matrix:

$$\begin{aligned} a &= \frac{1}{2} + \frac{4\tau_a C_a\,(C_b + n_{\mathrm{th}})}{(1 + C_a - C_b)^2}, \\ b &= \frac{1}{2} + \frac{4\tau_b C_b\,(C_a + n_{\mathrm{th}} + 1)}{(1 + C_a - C_b)^2}, \\ c &= \frac{2\,(C_a + C_b + 2n_{\mathrm{th}} + 1)\,\sqrt{\tau_a\tau_b C_a C_b}}{(1 + C_a - C_b)^2}. \end{aligned} \tag{C9}$$

APPENDIX D: CONVERTING OPTICAL-MICROWAVE ENTANGLEMENT INTO MICROWAVE-MICROWAVE ENTANGLEMENT

This appendix provides the procedure for calculating the MM covariance matrix from the MO covariance matrices for both the down-conversion and swapping classes of networks. For the entanglement-distribution case, the optical mode of the MO state is down-converted and the covariance matrix of the resulting MM state is found using

$$\mathbf{V}_{\mathrm{MM}} = (\mathbf{T}_d \oplus \mathbf{I}_2)\,\mathbf{V}_{\mathrm{OM}}\,(\mathbf{T}_d \oplus \mathbf{I}_2)^{\top} + \mathbf{N}_d \oplus 0\mathbf{I}_2. \tag{D1}$$

For the entanglement-swapping case, we start with two MO states both having a covariance matrix of the form of Eq. (C3). After measuring the optical mode of each state via a joint EPR measurement, the covariance matrix of the resulting MM state is given by [26]

$$\mathbf{V}_{ij} = \begin{pmatrix} \left(b_i - \frac{c_i^2}{a_i + a_j}\right)\mathbf{I}_2 & -\frac{c_i c_j}{a_i + a_j}\mathbf{Z}_2 \\ -\frac{c_i c_j}{a_i + a_j}\mathbf{Z}_2 & \left(b_j - \frac{c_j^2}{a_i + a_j}\right)\mathbf{I}_2 \end{pmatrix}, \tag{D2}$$

where the subscript on $\mathbf{V}$ indicates which states go into the swapping measurement. For the symmetric swapping case (where both MO states are identical), the MM covariance matrix reduces to

$$\mathbf{V}_{ii} = b_i\,\mathbf{I}_4 - \frac{c_i^2}{2a_i}\begin{pmatrix} \mathbf{I}_2 & \mathbf{Z}_2 \\ \mathbf{Z}_2 & \mathbf{I}_2 \end{pmatrix}. \tag{D3}$$

APPENDIX E: THRESHOLDS AND LOGARITHMIC NEGATIVITY

The entanglement of a 1×1 balanced-correlated Gaussian state with covariance matrix of the form of Eq. (C3) can be quantified using the minimum symplectic eigenvalue of the partially transposed covariance matrix (MSEPTCM), which is easily calculated using [28]

$$\tilde{\nu} = \frac{a + b - \sqrt{(a-b)^2 + 4c^2}}{2}. \tag{E1}$$

A state with a covariance matrix of the form given in Eq. (C3) is entangled if and only if $\tilde{\nu} < \frac{1}{2}$. The logarithmic negativity is easily calculated from the MSEPTCM using

$$E = \max\left\{0, -\log_2(2\tilde{\nu})\right\}. \tag{E2}$$

Our network-entanglement thresholds are found by solving the inequality $\tilde{\nu} < \frac{1}{2}$ for n_{th}. We then maximize these upper bounds on n_{th} and the logarithmic negativities subject to the following constraints on cooperativities:

$$0 \le C_{a,i} \le D_a, \tag{E3}$$

$$0 \le C_{b,i} \le D_b, \tag{E4}$$

$$\textit{IO 1:}\quad C_a < C_b + 1, \tag{E5}$$

$$\textit{IO 2:}\quad \frac{4G_a^2}{\kappa_b + \gamma_m} < \frac{4G_b^2}{\kappa_a + \gamma_m} + \kappa_a + \kappa_b, \tag{E6}$$

$$\textit{IM 1:}\quad C_b < C_a + 1, \tag{E7}$$

$$\textit{IM 2:}\quad \frac{4G_b^2}{\kappa_a + \gamma_m} < \frac{4G_a^2}{\kappa_b + \gamma_m} + \kappa_a + \kappa_b, \tag{E8}$$

where i indexes the transducer (since there are two in a network) and $D_{\{a,b\}}$ is the maximum achievable optical or microwave cooperativity, respectively. This replicates the ability experimentally to tune a cooperativity to the optimal value by controlling pump power. The first two equations apply to all transducers, whereas the last four equations are stability constraints that only apply to transducers operating as intrinsic optical or microwave entanglement sources.

APPENDIX F: EXTENDED DISCUSSION OF THRESHOLDS

Returning to the symbolic expressions for the network-entanglement thresholds given in Table I, we note that only the extrinsic optical thresholds depend on the squeezing parameter r. For the extrinsic optical down-conversion topology, this is because both modes of the TMS state experience decoherence (due to transduction). As mentioned in the main text, the extrinsic optical swapping topology behaves similarly to the extrinsic optical down-conversion topology, which is why its threshold also depends on r. In contrast, the extrinsic microwave topologies do not depend on r, because one mode of each squeezed resource does not experience any decoherence. The intrinsic topologies do not utilize an extrinsic squeezing resource and thus their thresholds do not depend on the squeezing parameter r.

There is not a set of parameter values for which the extrinsic microwave topologies are optimal in terms of the network-entanglement thresholds. However, the extrinsic microwave topologies may still be optimal with respect to logarithmic negativity. Additionally, the extrinsic microwave topologies are the only topologies for which setting all cooperativities to their maximum stable values is not optimal in terms of the network-entanglement threshold.

A straightforward way to use two transducers to transfer a quantum state is to simply up-convert the state, send it over the optical channel, and then down-convert the state. This is sometimes referred to as the "pitch-and-catch" protocol. We note that the Choi state corresponding to this quantum channel is the microwave-microwave state produced by the extrinsic microwave down-conversion topology in the limit $r \to \infty$. Therefore, the threshold given in Table I for the extrinsic microwave down-conversion topology also represents the entanglement-breaking threshold for this pitch-and-catch channel. When this inequality is not satisfied, then the pitch-and-catch channel is equivalent to a classical measure-and-prepare channel.

APPENDIX G: ASYMMETRIC GAUSSIAN ENTANGLEMENT SWAPPING OF BALANCED-CORRELATED GAUSSIAN STATES IS NEVER OPTIMAL

Let $\mathbf{V}_1$ and $\mathbf{V}_2$ be two distinct ($\mathbf{V}_1 \neq \mathbf{V}_2$) two-mode balanced-correlated Gaussian states with covariance matrices given by Eq. (C3). Suppose that we perform an EPR measurement on the first mode of each state (i.e., the positive operator-valued measure (POVM) elements are infinitely squeezed displaced two-mode squeezed states).

Theorem.—Let the MSEPTCM of the resulting state be $\tilde{\nu}_{ij}$ where $i,j \in \{1,2\}$ index which states were used in the swapping protocol. Then

$$\min\{\tilde{\nu}_{11}, \tilde{\nu}_{22}\} \leq \tilde{\nu}_{12}. \tag{G1}$$

Alternatively, stated in terms of logarithmic negativity [Eq. (E2)], this is

$$E_{12} \leq \max\{E_{11}, E_{22}\}. \tag{G2}$$

Proof.—The MSEPTCM for the asymmetric swapping case can be found by using Eqs. (D2) and (E1) and, explicitly, is

$$\tilde{\nu}_{12} = \frac{1}{2}\left[b_1 + b_2 - \frac{c_1^2 + c_2^2 + \sqrt{4c_1^2c_2^2 + X^2}}{a_1 + a_2},\right], \tag{G3}$$

where, for convenience, we introduce the quantity $X = \big((b_1 - b_2)(a_1 + a_2) - c_1^2 + c_2^2\big)$. The MSEPTCM for the two symmetric swapping cases can be found by using Eqs. (D3) and (E1) and, explicitly, is

$$\tilde{\nu}_{ii} = b_i - \frac{c_i^2}{a_i}. \tag{G4}$$

We show that $\min\{\tilde{\nu}_{11}, \tilde{\nu}_{22}\} \leq \tilde{\nu}_{12}$ and, without loss of generality, we can take $\tilde{\nu}_{11} \leq \tilde{\nu}_{22}$. What we want to prove is then $\tilde{\nu}_{11} \leq \tilde{\nu}_{12}$, which is equivalent to

$$b_1 - \frac{c_1^2}{a_1} \leq \frac{1}{2}\left[b_1 + b_2 - \frac{c_1^2 + c_2^2 + \sqrt{4c_1^2c_2^2 + X^2}}{a_1 + a_2}\right]. \tag{G5}$$

With some algebra, this reduces to

$$\left[2\frac{a_2}{a_1}c_1^2 - X\right] \geq \sqrt{4c_1^2c_2^2 + X^2}. \tag{G6}$$

The left-hand side of this equation is non-negative, which we show momentarily. Therefore, we can proceed to square both sides of Eq. (G6), so that we have

$$\left[2\frac{a_2}{a_1}c_1^2 - X\right]^2 \geq 4c_1^2c_2^2 + X^2, \tag{G7}$$

$$a_2^2c_1^2 - a_2a_1X \geq a_1^2c_2^2, \tag{G8}$$

$$a_1(b_2a_2 - c_2^2) \geq a_2(b_1a_1 - c_1^2), \tag{G9}$$

which is equivalent to the statement $\tilde{\nu}_{11} \leq \tilde{\nu}_{22}$, which is true.

Now the only thing left to show is that left-hand side of Eq. (G6) is non-negative. To prove that the left-hand side is non-negative, we need to show

$$-(b_1 - b_2) + 2\frac{c_1^2}{a_1} - \frac{c_1^2 + c_2^2}{a_1 + a_2} \geq 0, \tag{G10}$$

$$2\frac{c_1^2}{a_1} - \frac{c_1^2 + c_2^2}{a_1 + a_2} \geq b_1 - b_2. \tag{G11}$$

Now, since $a_i \geq 1/2$ and $c_i^2 \geq 0$, the following inequality is true:

$$\frac{c_1^2a_2}{a_1} + \frac{c_2^2a_2}{a_2} \geq 0. \tag{G12}$$

With some algebraic steps, this can be brought into the form

$$c_1^2 + \frac{c_1^2 a_2}{a_1} + c_2^2 + \frac{c_2^2 a_2}{a_2} \geq c_1^2 + c_2^2, \tag{G13}$$

$$\frac{c_1^2(a_1+a_2)}{a_1} + \frac{c_2^2(a_1+a_2)}{a_2} \geq c_1^2 + c_2^2, \tag{G14}$$

$$\frac{c_1^2}{a_1} + \frac{c_2^2}{a_2} \geq \frac{c_1^2+c_2^2}{a_1+a_2}, \tag{G15}$$

$$2\frac{c_1^2}{a_1} - \frac{c_1^2+c_2^2}{a_1+a_2} \geq \frac{c_1^2}{a_1} - \frac{c_2^2}{a_2}. \tag{G16}$$

Now we use our choice of $\tilde{\nu}_{11} \leq \tilde{\nu}_{22}$, which can be stated as

$$\frac{c_1^2}{a_1} - \frac{c_2^2}{a_2} \geq b_1 - b_2. \tag{G17}$$

This, together with the inequality given in Eq. (G16), proves that the inequality in Eq. (G11) is true. Therefore the left-hand side of the inequality in Eq. (G6) is always non-negative. Thus we show that entanglement swapping between distinct two-mode balance-correlated Gaussian states always produces less entanglement than swapping identical copies of one of these two-mode states. ■

APPENDIX H: DISTRIBUTING A FIXED AMOUNT OF EXTERNAL OPTICAL LOSS

Sections III D and V introduce external optical transmission loss via the transmissivity parameter τ_e, which must be included as a parameter in the optimization procedure for each network topology. Specifically, for the topologies that have more than one distinct optical mode, which include all the swapping topologies [Figs. 2(d)–2(f)] along with the extrinsic optical down-conversion topology [Fig. 2(a)], we assume that there is the ability to split this loss up arbitrarily between the optical modes. As the extrinsic microwave down-conversion [Fig. 2(b)] and intrinsic optical or microwave down-conversion [Fig. 2(c)] topologies only have one optical mode, there is no freedom to distribute this between modes, as it all must be incurred along the transmission of the single involved optical mode. The extrinsic optical swapping topology is the only topology that involves four optical modes and so one may consider distributing τ_e arbitrarily between all four modes. However, Ref. [26] shows that this scenario of entanglement swapping of two TMS states with some fixed loss that can be distributed among the modes cannot result in a lower effective loss than when simply distributing one TMS state with the same fixed loss. Thus extrinsic optical down-conversion will always perform at least as well as extrinsic optical swapping, even with this additional freedom in distributing τ_e among all the optical modes. In the following subsections, we prove several results concerning the optimal way to distribute τ_e in certain scenarios.

1. Equal distribution of loss is optimal for extrinsic optical down-conversion

Here, we consider the extrinsic optical down-conversion scenario [Fig. 2(a)], where we now have some fixed external loss that can be freely distributed between the optical modes before down-conversion. We prove that distributing this loss equally onto the two optical modes maximizes the logarithmic negativity of the MM state after down-conversion of both optical modes. We apply loss with transmissivity parameters τ_1 and τ_2 to each of the two modes of a TMS state with a covariance matrix given by Eq. (C1). We then apply the down-conversion channel, which is given by Eq. (A6), to each mode. The final MM state then has a covariance matrix of the form given by Eq. (C3), with

$$\begin{aligned} a &= \tau_d\left(\tau_1 \sinh^2(r) + \frac{1}{2}\right) + n_d, \\ b &= \tau_d\left(\tau_2 \sinh^2(r) + \frac{1}{2}\right) + n_d, \\ c &= \frac{1}{2}\tau_d\sqrt{\tau_1\tau_2}\sinh(2r). \end{aligned} \tag{H1}$$

Computing the MSEPTCM using Eq. (E1) gives

$$\tilde{\nu}(\tau_1,\tau_2) = n + \frac{\tau_d}{2}\left(1 - Y\sinh\, r\right), \tag{H2}$$

where for compactness we introduce the quantity

$$Y = \sqrt{(\tau_1+\tau_2)^2\sinh^2(r) + 4\tau_1\tau_2} - (\tau_1+\tau_2)\sinh\, r, \tag{H3}$$

which we note is always positive.

To find when the logarithmic negativity is maximized with respect to τ_1 and τ_2, we then compute

$$\frac{d\tilde{\nu}(\tau_1,\tau_e/\tau_1)}{d\tau_1} = \frac{\tau_d\left(\tau_1^2-\tau_e\right)Y\sinh^2(r)}{2\tau_1\left(Y+(\tau_1+\tau_2)\sinh\, r\right)}. \tag{H4}$$

So we see that with respect to $\tau_1 \in [\tau_e, 1]$, $\tilde{\nu}$ is maximized for $\tau_1 = \tau_e, \tau_2 = 1$ or $\tau_1 = 1, \tau_2 = \tau_e$, while it is minimized for $\tau_1 = \tau_2 = \sqrt{\tau_e}$. Thus equally distributing some fixed loss characterized by total transmissivity τ_e onto each mode maximizes the logarithmic negativity in the extrinsic optical down-conversion scenario.

2. Completely unequal distribution of loss is optimal for symmetric swapping

Here, we consider the situation where, given two copies of a MO balanced-correlation state [covariance matrix

given in Eq. (C3)], the optical modes experience some fixed amount of transmission loss before the swapping measurement. If there is the freedom to distribute this fixed amount of loss between the optical modes prior to the joint measurement, we prove that putting all the loss into one of the modes maximizes the logarithmic negativity of the MM state resulting from entanglement swapping.

After incurring some optical loss with transmissivity parameter τ_i, the balanced-correlation covariance matrix of the MO state is given by

$$\mathbf{V}_i = \begin{pmatrix} \tau_i a + (1-\tau)/2\ \mathbf{I}_2 & \sqrt{\tau_i} c\ \mathbf{Z}_2 \\ \sqrt{\tau_i} c\ \mathbf{Z}_2 & b\ \mathbf{I}_2 \end{pmatrix}. \tag{H5}$$

Now consider performing entanglement swapping on the optical modes of two of these states, $\mathbf{V}_1$ and $\mathbf{V}_2$, where each incurs some potentially different loss with transmissivity parameters τ_1 and τ_2, respectively, but fixing the total loss incurred before swapping by setting $\tau_1\tau_2 = \tau_e$. Using Eq. (G3), the MSEPTCM after swapping is given by

$$\tilde{\nu}(\tau_1, \tau_2) = \frac{(\tau_1+\tau_2)(b(a-1/2)-c^2)+b}{(\tau_1+\tau_2)(a-1/2)+1}. \tag{H6}$$

To find when the logarithmic negativity is maximized with respect to τ_1 and τ_2, we compute

$$\frac{d\tilde{\nu}(\tau_1, \tau_e/\tau_1)}{d\tau_1} = \frac{c^2\left(\tau_e - \tau_1^2\right)}{\left(\left(\tau_e - \tau_1^2\right)(a-1/2)+\tau_1\right)^2}. \tag{H7}$$

So we see that with respect to $\tau_1 \in [\tau_e, 1]$, $\tilde{\nu}$ is minimized for $\tau_1 = \tau_e, \tau_2 = 1$ or $\tau_1 = 1, \tau_2 = \tau_e$, while it is maximized for $\tau_1 = \tau_2 = \sqrt{\tau_e}$. Thus a completely asymmetric distribution of some fixed loss characterized by total transmissivity τ_e onto one or the other mode in symmetric swapping maximizes the logarithmic negativity.

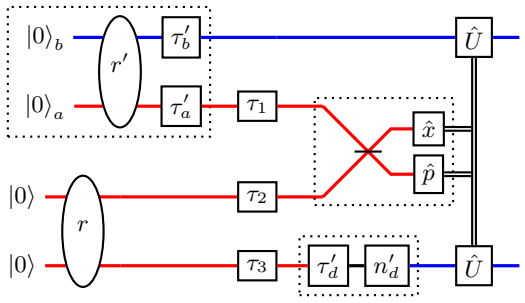

FIG. 6. A diagram of the microwave-microwave entanglement distribution topology, consisting of the asymmetric swapping of an intrinsic microwave and extrinsic optical microwave-optical entangled state. The transmissivities τ_1, τ_2, and τ_3 illustrate the optical modes where some total external optical transmission loss, $\tau_e = \tau_1\tau_2\tau_3$, could be freely distributed. In the main text, we rule out asymmetric swapping topologies such as this one by using the result shown in Appendix G. However, Fig. 7 shows that when allowing some external optical loss, this topology becomes optimal for some network-parameter values and τ_e, where in that plot $\tau_e = \tau_3$.

3. Asymmetric swapping potentially optimal with external optical loss

The nonoptimality of asymmetric swapping proven in Appendix G does not account for external optical loss. We find that introducing τ_e means that this result no longer holds. In fact, we give an explicit counterexample for the realistic device parameter values used in Sec. V, where the asymmetric topology consisting of swapping the intrinsic microwave (IM) and extrinsic optical (EO) MO states results in larger logarithmic negativity than the symmetric swapping of either IM or EO states. This asymmetric swapping topology is illustrated Fig. 6. Figure 7 shows an enlargement of an area of Fig. 5 in the main text where this counterexample can be seen. In this asymmetric swapping

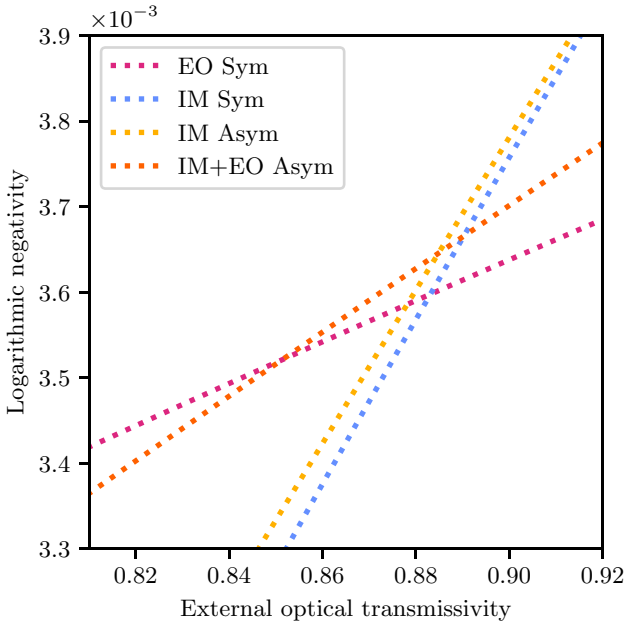

FIG. 7. The logarithmic negativity of the final microwave-microwave state generated by the network topology using recently reported electro-optomechanical-transducer parameter values, plotted as a function of optical loss external to the transducer. This figure shows an enlargement of a region of Fig. 5 in the main text. The extrinsic optical swapping ("EO Sym") and intrinsic microwave swapping ("IM Sym") are the same curves from Fig. 5. The "IM Asym" curve shows the completely asymmetric distribution of the external optical loss for the intrinsic microwave (IM) swapping (shown to be optimal for this topology in Appendix H 2. The "IM+EO Asym" curve shows the asymmetric swapping of an IM and EO MO state (illustrated in Fig. 6), where all external loss is put onto the down-converted optical mode. We assume 10 dB of extrinsic squeezing in for the EO topologies.

case, there are three optical modes over which τ_e may be distributed and in this particular case we find that it is optimal to put all of the external optical loss onto the down-converted optical mode of the EO MO state. We suspect that there may be asymmetric swapping scenarios in which it is optimal to not distribute all of τ_e onto one of the optical modes but put some amount τ_1 onto one mode and τ_2 onto the other, where τ_1 and τ_2 are not necessarily equal.

[1] X. Han, W. Fu, C.-L. Zou, L. Jiang, and H. X. Tang, Microwave-optical quantum frequency conversion, Optica **8**, 1050 (2021).

[2] C. L. Rau, A. Kyle, A. Kwiatkowski, E. Shojaee, J. D. Teufel, K. W. Lehnert, and T. Dennis, Entanglement Thresholds of Doubly Parametric Quantum Transducers, Phys. Rev. Appl. **17**, 044057 (2022).

[3] R. D. Delaney, M. D. Urmey, S. Mittal, B. M. Brubaker, J. M. Kindem, P. S. Burns, C. A. Regal, and K. W. Lehnert, Superconducting-qubit readout via low-backaction electro-optic transduction, Nature **606**, 489 (2022).

[4] M. Mirhosseini, A. Sipahigil, M. Kalaee, and O. Painter, Superconducting qubit to optical photon transduction, Nature **588**, 599 (2020).

[5] K. Stannigel, P. Rabl, A. S. Sørensen, P. Zoller, and M. D. Lukin, Optomechanical Transducers for Long-Distance Quantum Communication, Phys. Rev. Lett. **105**, 220501 (2010).

[6] K. Stannigel, P. Rabl, A. S. Sørensen, M. D. Lukin, and P. Zoller, Optomechanical transducers for quantum-information processing, Phys. Rev. A **84**, 042341 (2011).

[7] S. Krastanov, H. Raniwala, J. Holzgrafe, K. Jacobs, M. Lončar, M. J. Reagor, and D. R. Englund, Optically Heralded Entanglement of Superconducting Systems in Quantum Networks, Phys. Rev. Lett. **127**, 040503 (2021).

[8] J. Agustí, Y. Minoguchi, J. M. Fink, and P. Rabl, Long-distance distribution of qubit-qubit entanglement using Gaussian-correlated photonic beams, Phys. Rev. A **105**, 062454 (2022).

[9] B. Zhang, J. Wu, L. Fan, and Q. Zhuang, Hybrid Entanglement Distribution between Remote Microwave Quantum Computers Empowered by Machine Learning, Phys. Rev. Appl. **18**, 064016 (2022).

[10] M. Abdi, P. Tombesi, and D. Vitali, Entangling two distant non-interacting microwave modes, Ann. Phys. **527**, 139 (2014).

[11] S. R. Hedemann and B. D. Clader, Optomechanical entanglement of remote microwave cavities, J. Opt. Soc. Am. B **35**, 2509 (2018).

[12] C. Zhong, X. Han, and L. Jiang, Microwave and Optical Entanglement for Quantum Transduction with Electro-Optomechanics, Phys. Rev. Appl. **18**, 054061 (2022).

[13] S. Tserkis and T. C. Ralph, Quantifying entanglement in two-mode Gaussian states, Phys. Rev. A **96**, 062338 (2017).

[14] B. Kraus and J. I. Cirac, Discrete Entanglement Distribution with Squeezed Light, Phys. Rev. Lett. **92**, 013602 (2004).

[15] R. Horodecki, P. Horodecki, M. Horodecki, and K. Horodecki, Quantum entanglement, Rev. Mod. Phys. **81**, 865 (2009).

[16] G. Adesso and F. Illuminati, Gaussian measures of entanglement versus negativities: Ordering of two-mode Gaussian states, Phys. Rev. A **72**, 032334 (2005).

[17] R. F. Werner and M. M. Wolf, Bound Entangled Gaussian States, Phys. Rev. Lett. **86**, 3658 (2001).

[18] G. Vidal and R. F. Werner, Computable measure of entanglement, Phys. Rev. A **65**, 032314 (2002).

[19] C. Weedbrook, S. Pirandola, R. García-Patrón, N. J. Cerf, T. C. Ralph, J. H. Shapiro, and S. Lloyd, Gaussian quantum information, Rev. Mod. Phys. **84**, 621 (2012).

[20] L. Tian, Robust Photon Entanglement via Quantum Interference in Optomechanical Interfaces, Phys. Rev. Lett. **110**, 233602 (2013).

[21] E. X. DeJesus and C. Kaufman, Routh-Hurwitz criterion in the examination of eigenvalues of a system of nonlinear ordinary differential equations, Phys. Rev. A **35**, 5288 (1987).

[22] J. Eisert, S. Scheel, and M. B. Plenio, Distilling Gaussian States with Gaussian Operations is Impossible, Phys. Rev. Lett. **89**, 137903 (2002).

[23] G. Giedke and J. I. Cirac, Characterization of Gaussian operations and distillation of Gaussian states, Phys. Rev. A **66**, 032316 (2002).

[24] L.-M. Duan, G. Giedke, J. I. Cirac, and P. Zoller, Entanglement Purification of Gaussian Continuous Variable Quantum States, Phys. Rev. Lett. **84**, 4002 (2000).

[25] A. Kwiatkowski, E. Shojaee, S. Agrawal, A. Kyle, C. L. Rau, S. Glancy, and E. Knill, Constraints on Gaussian error channels and measurements for quantum communication, Phys. Rev. A **107**, 042604 (2023).

[26] J. Hoelscher-Obermaier and P. van Loock, Optimal Gaussian entanglement swapping, Phys. Rev. A **83**, 012319 (2011).

[27] B. Brubaker, J. Kindem, M. Urmey, S. Mittal, R. Delaney, P. Burns, M. Vissers, K. Lehnert, and C. Regal, Optomechanical Ground-State Cooling in a Continuous and Efficient Electro-Optic Transducer, Phys. Rev. X **12**, 021062 (2022).

[28] S. Pirandola, A. Serafini, and S. Lloyd, Correlation matrices of two-mode bosonic systems, Phys. Rev. A **79**, 052327 (2009).